

1 Supplement Svensson et al. Deposition of light-absorbing particles in glacier snow of the
2 Sunderdhunga Valley, the southern forefront of Central Himalaya

3

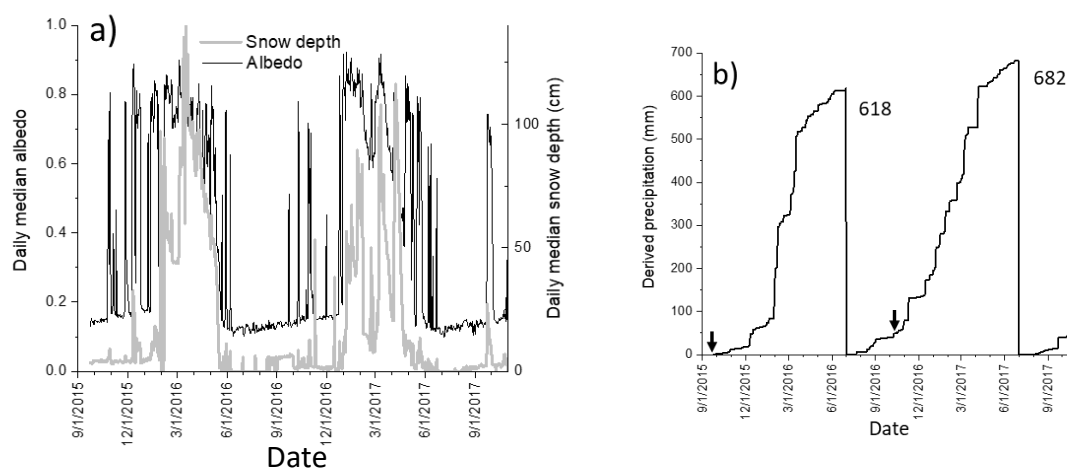
4 Snow depth and albedo with AWS

5 Albedo data processing: first, the SW radiation baselines values were adjusted to, $+10$ and $+2.5 \text{ W m}^{-2}$
6 for incoming and outgoing radiation, respectively. Second, incoming SW radiation had to be equal or
7 greater than outgoing SW radiation. This filter mainly removes noisy data during the dark period of the
8 day, but also episodes when the sensors are potentially covered by snow. Third, an albedo value of 0.2
9 was used to distinguish bare conditions from periods where there is sufficient amount of snow on the
10 ground.

11 Snow depth data processing: the last adjustment to the AWS data is related to the maximum snow depth
12 (SD) that is nominally achievable. The sensor is determined to be at a level of 192 cm above the ground
13 surface. The sensor should have at least a distance of 0.5 m between the sensor and the snow surface.
14 Hence, practically the maximum SD is 142 cm. However, we have used data up to 156 cm. At this SD
15 we note a clear change in response and the sensor have obvious difficulties to determine SD. On a few
16 instances, the SD depth is negative while there is obviously a thick snow cover. We suspect that this is
17 due to snow depth greater than 156 cm and that the sending and receiving of pulses is not synchronized
18 and interpreted as negative snow depths. For these limited periods, we have added the absolute value
19 of the negative snow depth to 156 cm if at the same time the snow albedo is at least 0.6 and the new SD
20 does not exceed 190 cm. This last adjustment improves the consistency between snow albedo and SD
21 but does little to the accumulated snow estimates.

22 Averaging: finally, we applied a moving 24 hour median filter to all the AWS data.

23



24

25

26 Figure S1. In a) the daily median snow depth is plotted together with the daily median albedo. In b) the
27 integrated positive changes in the snow depth is converted to precipitation assuming a snow density of
28 0.1 g m^{-3} . On 1 July, the integration is reset to zero. The integrated precipitation amounts for the two

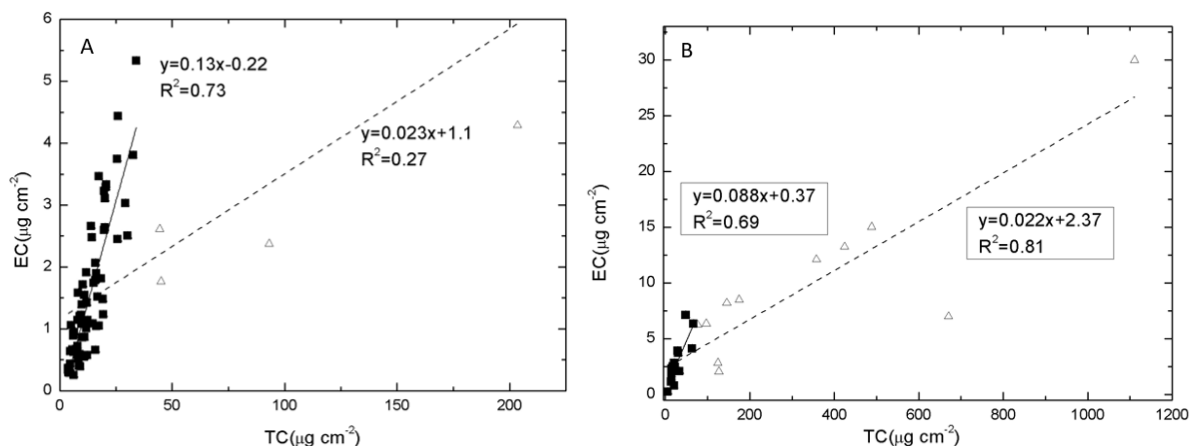
29 annual cycles are indicated in the figure. The time of sampling in 2015 and 2016 are indicated by the
30 small arrows.

31
32
33
34

35 TC/EC relationship, and more specifically, how linear relationships were established

36 First, a plot of EC as a function of TC containing the 2016 filter samples where the EC amounts were
37 assumed to be reliable (i.e. excluding the 17 samples where accurate EC determinations could not be
38 done) is presented in S2a with the slope of 0.023. In this plot it was evident that some outliers were
39 present in the data set, indicated by triangles in S2a. With these outliers removed in Fig. S2a, we
40 obtained the slope 0.13 (for all black squares). Using a similar approach for the 2015 filter samples
41 (S2b), we first obtained a slope of 0.022, and then a plot where samples that had a TC amount that was
42 higher than 70 μg was removed, yielding a slope of 0.088. Grouping the filtered data points from 2015
43 and 2016 together, we obtained the linear fit $EC = 0.10TC + 0.12$. This linear fit was applied to the
44 samples where EC was reconstructed.

45



46

47 Figure S2. EC TC ratio for (a) 2016 filter samples and (b) for 2015 filter samples.

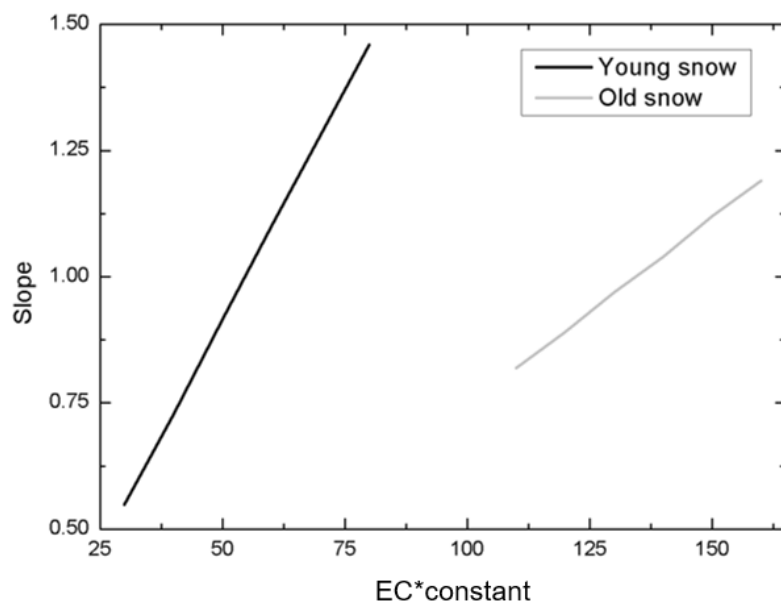
48

49

50 Determining the common effective constants for Young and Old snow (EC_y^* and EC_o^*), respectively.

51 In order to define the constants EC_y^* and EC_o^* we systematically changed the constant over a range of
52 values and plotted the slope returned for a linear fit between observed EC_{acc} and calculated EC_{acc}
53 using a particular constant. Where the linear fit returns a slope around 1, will be the candidate for the
54 constant value used in this study. Evident in Fig. S3, the EC_y^* constant is slightly more than $50 \mu\text{g L}^{-1}$,

55 while the EC_o^* constant was somewhat lower than $150 \mu\text{g L}^{-1}$. For convenience we chose to work with
56 the numbers 50 and 150 for EC_y^* and EC_o^* , respectively.



57
58 Figure S3. Different constants EC_y^* and EC_o^* and their corresponding slopes returned from linear fits
59 between observed and calculated EC_{acc} .

60